# Newly synthesized lipid-porphyrin conjugates: evaluation of their self assembling properties, their miscibility with phospholipids and their photodynamic activity in vitro

Julien Massiot, Véronique Rosilio, Nada Ibrahim, Akihisa Yamamoto, Valérie Nicolas, Oleg Konovalov, Motomu Tanaka, Ali Makky

# Newly synthesized lipid-porphyrin conjugates: evaluation of their self assembling properties, their miscibility with phospholipids and their photodynamic activity *in vitro*

Julien Massiot[a], Véronique Rosilio[a], Nada Ibrahim[a], Akihisa Yamamoto[b], Valérie Nicolas[c], Oleg Konovalov[d], Motomu Tanaka[b,e], Ali Makky[a]*

[a] Institut Galien Paris Sud, Univ Paris-Sud, CNRS, Université Paris-Saclay, 92296 Châtenay-Malabry, France
[b] Center for Integrative Medicine and Physics, Institute for Advanced Study, Kyoto University, 606-8501 Kyoto, Japan
[c] UMS IPSIT, Univ Paris-Sud, US 31 INSERM, UMS 3679 CNRS, 92290 Châtenay-Malabry, France
[d] European Synchrotron Radiation Facility (ESRF), Grenoble Cedex 9 38053, France
[e] Physical Chemistry of Biosystems, Physical Chemistry Institute, University of Heidelberg, 69120 Heidelberg, Germany
* Corresponding author: ali.makky@u-psud.fr

# Abstract

Lipid-porphyrin conjugates are considered nowadays as promising building blocks for the conception of supramolecular structures with multifunctional properties, required for efficient cancer therapy by photodynamic therapy (PDT). Herein, we report on the synthesis of two new lipid-porphyrin conjugates coupling pheophorbide-a (Pheo-a), a photosensitizer derived from chlorophyll-a, to either chemically modified milk lyso-phosphatidylcholine (PhLPC) or egg lyso-sphingomyelin (PhLSM). We investigated the impact of the lipid backbone of these conjugates on their self-assembling properties, as well as on their physicochemical properties, including interfacial behavior at the air/buffer interface, fluorescence and absorption properties, thermotropic behavior and incorporation rate in the membrane of liposomes. Finally, their photodynamic activity was evaluated on esophageal squamous cell carcinoma (ESCC) and

normal esophageal squamous epithelium cell lines. The liposome-like vesicles resulting from self-assembling of the pure conjugates were unstable and turned to aggregates with undefined structure within few days. However, both lipid-porphyrin conjugates could be efficiently incorporated in lipid vesicles, with higher loading rates than unconjugated Pheo-a. Interestingly, phototoxicity tests of free and liposome-incorporated lipid-porphyrin conjugates demonstrated a better selectivity *in vitro* to esophageal squamous cell carcinoma relative to normal cells.

# Introduction

Porphyrins are ubiquitous in geological and biological systems and are considered as the most abundant pigments in nature [1]. Depending on their chemical structure and on the nature of the metal chelated in their ring, they can play diverse important biological functions such as oxygen transport (heme), electron transport in cell respiration (cytochromes), photosynthesis (chlorophylls) and many other functions that are essentials for life [1]. Porphyrin pigments are thus called the "colors of life," since they are necessary to sustain key activities in nearly all organisms [1]. Added to these properties, porphyrins have received considerable attention as promising photosensitizers (PSs) for the treatment of small solid tumors by photodynamic therapy (PDT). Indeed, this latter consists in the combination of a photosensitizer, oxygen and harmless visible light at the appropriate wavelength to produce reactive oxygen species that can oxidize several vital biomolecules in cancerous cells and subsequently lead to cell death. Porfimer sodium (HpD, Photofrin ®) was the earliest porphyrin derivative employed in PDT [2] and was the first PS approved by FDA in 1995 for early stage lung cancer treatment [3]. Despite its high singlet oxygen quantum yield [4] and its efficiency in the treatment of different cancers, porfimer sodium has several drawbacks including weak light absorption in the phototherapeutic window and long-term cutaneous phototoxicity [5]. A large variety of photosensitizers have been

developed afterwards in order to minimize these drawbacks. Nevertheless, only few of them, such as temoporfin (*m*-THPC, Foscan®) and the benzoporphyrin derivative monoacid ring A (BPD-MA, verteporfin, Visudyne®) have been approved as PDT agents for the treatment of head and neck cancer [6] and age-related macular degeneration (AMD) [7], respectively. The poor water solubility of most of these porphyrin derivatives and their tendency to aggregate under physiological conditions are key limitations to the achievement of an efficient photodynamic activity. In fact, the hydrophobic nature of most photosensitizers makes their intravenous administration a difficult task. Furthermore, the monomeric state of PSs is required to maintain their photophysical, chemical and biological properties [8]. In addition to their water solubility issue, many photosensitizers display poor tumor selectivity [9]. In order to overcome these drawbacks, several strategies have been adopted during the last years, including porphyrin glycosylation [10], pegylation [11] and their incorporation into nanocarriers such as organic [12] and inorganic nanoparticles[12c, 13], and liposomes [7, 14]. Among these strategies, embedding PSs in liposomal bilayers seems to be the strategy of choice for several reasons. Indeed, liposomes are composed of biocompatible, biodegradable materials and can be easily produced at industrial scale, due to their simplicity and to lower investment costs compared to other nanoparticulate systems [15]. Added to these advantages, several studies have shown the efficiency of liposomes in improving the solubility and selectivity of PSs [16]. Indeed, the selective accumulation of liposomes in tumors is at least partially related to the leaky tumor vasculature which allows liposomes to extravasate across the leaky tumor vessels [17]. Despite these improvements, liposomal delivery systems showed low loading efficiency of PSs within their lipid bilayers and rapid clearance of PSs from the blood due to their transfer to serum components[16b, 18]. Thus, the focus on PS drug delivery has shifted recently towards the development of new nanocarriers composed of only one building block with self-assembly properties, allowing high PS payload,

and facilitating their clinical translation as well as their production at industrial scale [9]. To our best of knowledge, only one kind of such materials has been reported based on lipid-porphyrin conjugates. These building blocks have been synthesized by Gang Zheng's group [19] who discovered the efficiency of such compounds to self-assemble into liposome-like nanoparticles named "porphysomes" and possessing multifunctional properties, including photothermal therapy (PTT), photodynamic therapy (PDT), photo-triggered drug release and photoacoustic imaging (PAI) [19-20]. Thanks to their organic nature, porphysomes are enzymatically biodegradable and induce minimal acute toxicity during their retention in mice [19b]. These lipid-porphyrin conjugates were synthesized through esterification of the sn-2 position of lysophosphatidylcholine with either pyropheophorbide a or bacteriochlorophyll a [19b]. In addition, such conjugates may exhibit different localization into cell organelles compared to free porphyrins compounds[21]. Considering these advantages, we believe there is still considerable room for the development of new lipid-porphyrin conjugates, the study of their self-assembling properties and PDT efficiency. Thus, the aim of this work was to synthesize a new kind of lipid-porphyrin conjugates based on various lipid backbones linked to a PS via a peptidic bond instead of the ester bond used in porphysomes [19b, 20]. To do so, two new lipid-porphyrin conjugates were synthesized by coupling Pheo-a, a photosensitizer derived from chlorophyll-a, to either chemically modified milk lyso-phosphatidylcholine (lyso-PC) or egg lyso-sphingomyelin (lyso-eSM). The physicochemical properties of these compounds and their self-assembling properties were assessed, as well as their efficiency *in vitro* on esophageal squamous cell carcinoma (ESCC) cell lines.

# Material and methods

## Chemicals

Pheophorbide a (Pheo-a, ≥ 95%, mixture of diastereomers, Mw = 592.69 g/mol) was purchased from Frontier Scientific (Logan, UT), and 6-(Fmoc-amino)hexanoic acid (≥ 98%, Mw = 353.42 g/mol) from Novabiochem (Laufelfingen, Switzerland). N,N′-Dicyclohexylcarbodiimide (DCC, ≥ 99%, Mw = 206.33 g/mol), HATU (≥ 97%, Mw = 380.23 g/mol), 4-(Dimethylamino)pyridine (DMAP, ≥ 99%, Mw = 122.17 g/mol), Dowex® 50WX8-100 ion exchange resin (hydrogen form), N,N-Diisopropylethylamine (DIPEA, 99%, Mw = 129.24 g/mol), HEPES (99.5%, Mw = 238.31 g/mol), sodium chloride (NaCl, 99%, Mw = 58.44 g/mol), Ammonium molybdate(VI) tetrahydrate (81-83%, Mw = 1235.86 g/mol), L-Ascorbic acid (99%, Mw = 176.12 g/mol), 0.65 mM Phosphorus standard solution, hydrogen peroxide (30 wt %), chloroform anhydrous (≥99%, stabilized with amylenes) and methanolic hydrogen chloride (0.5N) were provided by Sigma (St. Louis, MO, USA).

The phospholipids 1-palmitoyl-2-hydroxy-sn-glycero-3-phosphocholine (16:0 Lyso PC, 99%, 495.63 g/mol), 1-stearoyl-2- oleoyl-sn-glycero-3-phosphocholine (SOPC, 99%, Mw = 788.14 g/mol), 1,2-distearoyl-sn-glycero-3-phosphocholine (DSPC, 99%, Mw = 790.15 g/mol), 1,2-distearoyl-sn-glycero-3-phosphoethanolamine-N-[methoxy(polyethyleneglycol)–2000]-ammonium salt (DSPE-mPEG$_{2000}$, 99%, Mw = 2805,497 g/mol) and egg sphingomyelin (Egg SM, 99%, Mw = 710.965) were purchased from Avanti Polar Lipids (Alabaster, AL). Chloroform, methanol and anhydrous N,N-dimethylformamide (DMF, 99.8% pure) were analytical-grade reagents purchased from Carlo Erba (Val de Reuil, France). The ultrapure water ($\gamma$ = 72.2 mN/m at 22° C) used in all experiments was produced by a Millipore Milli-Q® Direct 8 water purification System, with a resistivity of 18.2 MΩ.cm.

**Synthesis of compound 1**

16:0 Lyso PC (150 mg, 0.3 mmol) and Fmoc-6-Ahx-OH (212 mg, 0.6 mmol) were mixed in 5 ml of anhydrous chloroform and stirred until clear mixture was obtained. DMAP (110 mg, 0.9 mmol) and DCC (120 mg, 0.6 mmol) were added separately, in cold anhydrous chloroform. Glass beads (2 mm, previously washed with ethanol, and dried under vacuum) were added and the mixture was brought back to room temperature and sonicated for 8 hours. Temperature was kept under 25 °C. Fmoc-6-Ahx-OH (50 mg, 0.15 mmol) was added after 2, 4 and 6 hours of sonication. Once the 8 hours sonication were over, the mixture was stirred at room temperature for an additional 12 hours. It was then incubated with DOWEX (Dowex® 50WX8 hydrogen form) for 45 minutes to remove DMAP, filtered, and concentrated under vacuum until a white precipitate appeared. The 1-2 ml mixture was then centrifuged for 5 min at 2000 *g* and the yellow liquid crude mixture was purified by chromatography on silica gel (eluted with chloroform-methanol-water 65:25:4, volume ratio; Rf = 0.35-0.4). Pure compound 1 (207 mg, white powder, yield 83 %) was dried under vacuum, lyophilized overnight, and stored at -20 °C. NMR: $^{1}$H NMR ($CDCl_3$, 300 MHz) δ (ppm) 7.76 (d, 2H, *J* = 7.5 Hz), 7.61 (d, 2H, *J* = 7.1 Hz), 7.42 (m, 4H), 5.46 (br s, 1H), 5.23 (m, 1H), 4.38-4.10 (br m, 7H), 3.96 (br t, 2H), 3.77 (br m, 2H), 3.32 (s, 9H), 3.17 (m, 2H), 2.29 (m, 4H), 1.58 (m, 6H), 1.26 (br s, 26H), 0.89 (t, 3H, *J* = 6.5 Hz); $^{13}$C NMR ($CDCl_3$, 75 MHz) δ (ppm) 167.59, 165.52, 144.04, 141.26, 127.64, 127.03, 125.14, 119.93, 70.72, 66.33, 59.37,54.37,47.29, 40.81, 34.08, 31.91, 29.71 (br), 29.36 29.18, 26.11, 24.89, 22.68, 14.11. MS $(ESI)^+$ for $[C_{45}H_{72}N_2O_{10}P]^+$; calculated: 831.4925; observed: 831.4912.

**Synthesis of compound 2 (PhLPC)**

Compound 1 (133 mg, 0.16 mmol) was dissolved into 4 mL of DMF anhydrous, 2 mL of DIPEA and was stirred for 5 hours at room temperature to complete the full Fmoc deprotection. Pheo-a (95 mg, 0.16 mmol) and HATU (75 mg, 0.2 mmol) were combined in 4 ml of anhydrous DMF,

stirred for 1 hour at room temperature under Argon, in the dark, and then added to the deprotected compound 1. The mixture was stirred in the dark at room temperature, under Argon, for 24 hours. DMF was then removed under vacuum. The crude was resuspended in minimum amount of chloroform and purified by chromatography on silica gel (eluted with chloroform-methanol-water 65:25:4, volume ratio; Rf = 0.5). Compound 2 was obtained (120 mg, dark-green powder, yield 63 %). NMR: $^{1}$H NMR (DMSO-$d_6$, 400 MHz) δ (ppm) 9.34 (s, 1H), 8.93 (s, 1H), 8.80 (s, 1H), 7.86 (m, 1H), 6.40 (s, 1H), 6.15 (m, 1H), 6.03 (bd, 1H, *J* = 11.5 Hz), 5.01 (br s, 1H), 4.58 (d, 1H, *J* = 6.9 Hz), 4.19 (d, 2H, *J* = 9.3 Hz), 4.05 (br m, 3H), 3.86 (s, 3H), 3.72 (br m, 2H), 3.50 (m, 5H), 3.27 (br s, 5H), 3.13 (s, 9H), 2.91 (br m, 2H), 2.80 (s, 3H), 2.11 (br m, 6H), 1.81 (d, 3H, *J* = 6.9 Hz), 1.60 (m, 2H), 1.42 (m, 5H), 1.31 (m, 2H), 1.08 (m, 2H), 1.06-0.85 (br s, 26H), 0.706 (t, 3H, *J* = 7.1 Hz), 0.17 (s, 1H); $^{13}$C NMR (DMSO-$d_6$, 100 MHz) δ (ppm) 189.18, 173.05, 172.52, 172.23, 171.36, 169.27, 161.90, 154.43, 150.00, 148.70, 144.57, 141.30, 137.05, 135.72, 135.10, 131.89, 128.62 (CH), 128.26, 122.80, 105.21, 104.20 (CH), 96.48 (CH), 93.70 (CH), 70.57 (CH), 65.47, 64.30, 62.60, 62.33, 58.30, 53.10 (3x$CH_3$), 52.62 ($CH_3$), 51.30 (CH), 49.41 (CH), 38.26, 33.22, 32.47, 31.12, 28.78, 28.51, 28.24, 25.71, 24.24, 24.10, 22.82 ($CH_3$), 21.94, 18.31, 17.13 ($CH_3$), 13.77 ($CH_3$), 11.75 ($CH_3$), 11.53 ($CH_3$), 10.36 ($CH_3$). MS (MALDI-TOF)$^{+}$ for $[C_{65}H_{96}N_6O_{12}P]^{+}$; calculated: 1183.48; observed: 1183.66.

**Synthesis of compound 3**

Egg SM (400 mg, 0.56 mmol) was dissolved in anhydrous methanolic hydrogen chloride (40 mL, 0.5 M) in a sealed vessel, and stirred at 55 °C for 7 days. The crude mixture was then dried under vacuum, resuspended in minimum amount of chloroform-methanol (9:1), and purified by chromatography on silica gel (eluted with chloroform-methanol-water 65:25:4, volume ratio; Rf = 0.1). Compound 3 was obtained (165 mg, white powder, yield 65 %). NMR: $^{1}$H NMR (MeOD, 300 MHz) δ (ppm) 5.96-5.86 (m, 1H), 5.51 (dd, 1H, *J* = 15.2, 6.6 Hz), 4.33 (m, 2H), 4.08 (br m,

3H), 3.71 (br s, 2H), 3.40 (br s, 1H), 3.27 (s, 9H), 2.11 (m, 2H), 1.45 (br m, 2H), 1.30 (br s, 22H), 0.91 (t, 3H, *J* = 6.6 Hz); $^{13}$C NMR (MeOD, 75 MHz) δ (ppm) 137.29 (CH), 128.25 (CH), 70.66 (CH), 67.31, 56.92 (CH), 54.79 (3x$CH_3$), 33.45, 33.07, 30.80, 30.66, 30.46, 30.17, 23.74, 14.46 ($CH_3$); MS (ESI)$^+$ for $[C_{23}H_{50}N_2O_5P]^+$; calculated: 465.3457; observed: 465.3456).

**Synthesis of compound 4 (PhLSM)**

Pheo-a (160 mg, 0.27 mmol) and HATU (100 mg, 0.27 mmol) were mixed in 4 ml of anhydrous DMF and stirred for 1 hour at room temperature under Argon, in the dark. Compound 3 (115 mg, 0.25 mmol) was dissolved in anhydrous DMF with 0.5 ml of DIPEA, and then added to the Pheo a - HATU mixture, and stirred in the dark, at room temperature and under Argon for 24 hours. DMF was then removed under strong vacuum. The crude was resuspended in minimum amount of chloroform and purified by chromatography on silica gel (eluted with chloroform-methanol-ammonia 70:30:4, volume ratio; Rf = 0.3). Compound 4 was obtained (78 mg, white powder, yield 30 %). NMR: $^1$H NMR (DMSO-$d_6$, 400 MHz) δ (ppm) 9.51 (s, 1H), 9.11 (s, 1H), 8.82 (s, 1H), 7.96 (m, 1H), 6.61 (s, 1H), 6.38 (s, 1H), 6.18 (d, 1H, *J* = 18 Hz), 6.06 (m, 1H), 5.42 (br m, 1H), 5.26 (br m, 1H), 4.53 (br s, 1H), 4.05-4.01 (br m, 3H), 3.87 (br m, 1H), 3.83 (s, 3H), 3.57 (s, 3H), 3.52 (s, 2H), 3.44-3.40 (br, m, 4H), 3.31 (s, 3H), 3.11 (s, 9H), 2.95 (s, 3H), 2.14 (br, m, 2H), 1.75 (s, 3H), 1.59-1.61 (br, m, 3H), 1.50 (s, 3H), 1.20-0.50 (br, m, 27H); $^{13}$C NMR (DMSO-$d_6$, 100 MHz) δ (ppm) 189.34, 173.24, 169.59, 155.52, 154.57, 145.02, 141.55, 137.23, 136.04, 135.36, 132.07, 132.01, 131.03, 130.72, 128.80, 128.41, 123.09, 105.11, 104.46, 96.57, 93.79, 69.90, 65.51, 58.42, 54.53, 53.21, 52.66, 51.42, 49.76, 31.17, 30.88, 28.69, 22.82, 21.98, 21.84, 18.38, 17.28, 13.87, 11.93, 11.66, 10.60; MS (MALDI-TOF)$^+$ for $[C_{58}H_{84}N_6O_9P]^+$; calculated: 1039.60; observed: 1039.58.

**Surface pressure measurements**

Surface pressure-molecular area isotherms (π-A) of pure components or their mixtures with DSPC were recorded using a thermostated KSV-Nima Langmuir film balance (Biolin Scientific, Finland), composed of a teflon trough (775.75 $cm^2$) equipped with two 145 mm Delrin barriers. Pure components or mixtures in a chloroform/methanol (9:1) solution (4.0 x $10^{16}$ molecules) were spread onto the aqueous buffer solution (10 mM HEPES, 150 mM NaCl, pH = 7.4). After deposition, the solvents were allowed to evaporate for 15 min before compression of the monolayer at a rate of 5.0 Å²/molecule/min. All experiments were performed at 22.1 ± 0.7°C and the results reported are mean values of at least three measurements. From the surface pressure−area data, the surface compressional moduli K of monolayers were calculated, using Eq (1) with A the molecular area and dπ, the surface pressure change:

$$K = -A\left(\frac{d\pi}{dA}\right)_T \qquad \text{(Eq. 1)}$$

The excess free energy of mixing ($\Delta G^{EXC}$) of Pheo-a derivatives and DSPC was calculated according to Eq. (2):

$$\Delta G^{Exc} = \int_0^{\pi}(A_{12} - X_1A_1 - X_2A_2)d\pi \qquad \text{(Eq. 2)}$$

where $A_{12}$, $A_1$ and $A_2$ are the experimental molecular areas of the binary mixture and pure compounds, respectively. $X_1$ and $X_2$ are the molar fractions of the phospholipid and the photosensitizer, respectively. $\Delta G^{exc}$ values were plotted as a function of the monolayer composition, for surface pressures of 5, 10, 15, 20, 25 and 30 $mN.m^{-1}$.

**X-ray reflectivity experiments (XRR) at the air/buffer interface**

XRR experiments were carried out at the beamline ID10B of the European Synchrotron Radiation

Facility (ESRF, Grenoble). The samples were irradiated with a monochromatic synchrotron beam with an energy of 8 keV ($\lambda$ = 1.55 Å ). The XRR experiments were performed on monolayers of Pheo-a derivatives spread on the surface of HEPES buffer (HEPES 10 mM, KCl 150 mM, pH 7.4) and compressed to a surface pressure of 30 mN/m. The film balance was kept in a He atmosphere during the measurement to minimize the radiation damage. XRR was measured with a linear detector (Vantec-1, Bruker AXS, USA). After subtraction of the diffuse intensity background (at $\alpha_f \neq \alpha_i$), the specular reflectivity was analyzed using the Parratt formalism [22] with a genetic minimization algorithm implemented in the MOTOFIT software package [23].

**Differential scanning calorimetry (DSC)**

DSC measurements were carried out using a DSC Diamond Perkin-Elmer apparatus. Four scans of consecutive heating and cooling cycles between -10 °C and 15 °C were recorded to make sure that the thermal equilibrium was reached. Different scan rates were recorded, 5 °C/min (for the first two cycles), 2 °C/min and 1 °C/min. An empty pan was used as a reference. In addition, before each scan, a 2 min isotherm was recorded at the initial temperature to ensure that the samples were at thermal equilibrium. Multilamellar suspensions were prepared by hydration of a film made of SOPC-photosensitizer (97.5-2.5 mol %) with 45 µL of HEPES buffer (hydration rate of 90%). For each sample, a total mass of ~ 15 mg was placed in hermetically sealed aluminum pans. Samples were prepared in triplicate to check the reproducibility. To monitor the photooxidation of SOPC caused by the embedded photosensitizers, 50 µL of lamellar phase suspensions (5 mg SOPC) were illuminated for 14 min before starting the thermal measurements. Illumination was done with a homemade lamp composed of 4 Philips TL fluorescent tubes covered by a flat diffusing glass plate and fitted with an orange filter ($\lambda$ ~ 520–680 nm with a $\lambda_{max}$ = 590 nm) at a fluence of 2 J/cm$^{2}$,[24]. Calibration was carried out with pure cyclohexane (> 99.9% purity, 6.7 °C melting temperature) [25]. Data were collected and processed using Pyris

thermal analysis software (version 9.1). Phospholipid transition onset temperatures ($T_{on}$) were determined from the intercept of the baseline with the tangent to the left side of the peak.

**Preparation and characterization of liposomes and self-assembled structures**

Liposomes incorporating Pheo-a derivatives were prepared by the thin lipid film hydration method [26] followed by extrusion of the vesicles suspension. In brief, a mixture of DSPC (95 mol%), DSPE-mPEG2000 (2.5 mol%) and the studied photosensitizer (2.5 mol%) was prepared in chloroform:methanol (9:1 v/v). After removing the organic solvent under vacuum at 45 °C, the resulting film was rehydrated with 1 ml of DPBS to get a final 5 mM concentration of lipids. The mixture was vortexed and sonicated at 60 °C for 5 min. The suspension was then extruded 19 times through a 200 nm pore-sized polycarbonate membrane, while maintaining the temperature at 80 °C. The self-assembled structures were prepared following the same procedure after hydration of the lipid-porphyrin conjugate dry film with HEPES buffer. The hydrodynamic diameter and the zeta potential were measured by dynamic light scattering (DLS) (Nano ZS90, Malvern). All measurements were carried out at 25 °C. The mean diameter of the vesicles was 180 ± 10 nm, and their zeta potential was slightly negative (Table S3). The PS content in the liposome bilayers was evaluated by measuring the absorption of each liposomal sample, after disruption by addition of a methanol/THF mixture. PS loading efficiency (%) was determined as previously described [24].

**Cryo-TEM**

The self-assembled structures made of lipid-porphyrin conjugates were deposited on perforated carbon-coated, copper grid (TedPella, Inc) which was immediately plunged into a liquid ethane bath cooled with liquid nitrogen (180 °C) and then mounted on a cryo holder [27]. Cryo-Transmission electron microscopy (TEM) measurements were then performed using a JEOL

2200FS (JEOL USA, Inc., Peabody, MA, U.S.A.) working under an acceleration voltage of 200 kV (Institut Curie). Electron micrographs were recorded by a CCD camera (Gatan, Evry, France).

**Cell culture**

The immortalized esophageal squamous cell line HET-1A, used as a model for normal esophageal squamous epithelium, was purchased from the American Type Culture Collection (Manassas, VA) [28]. The human esophageal squamous cell carcinoma [29] Kyse-30 was obtained from Sigma Aldrich. Cells were grown in Roswell Park Memorial Institute (RPMI) 1640 medium supplemented with 10% fetal bovine serum (FBS), 100 IU/ml penicillin and 100 µg/ml streptomycin (GIBCO, Invitrogen) in a humidified incubator with 5% $CO_2$ at 37 °C. Cells were passaged every three days using 0.25% trypsin/ethylenediamine tetraacetic acid (EDTA) when confluence was at 70 to 80%.

**Cytotoxicity and phototoxicity studies**

Cells were seeded into 96-well plates (4000 cells, 100 µL cell culture medium per well) and incubated overnight in the humidified incubator. On the day of experiments, free porphyrin derivatives (in DMSO) or DSPC-porphyrin derivatives liposomes (in PBS buffer) at different concentrations were added to the wells in the dark. Each well contained a final volume of 200 µl of full medium. The final porphyrin concentrations ranged from 0 to 5 µM. Cells were incubated again for 24 hours to ensure full internalization of the porphyrin derivatives. The following day, the culture medium was replaced with fresh one. Cells were then either incubated in dark for cytotoxicity tests or illuminated for 14 min for phototoxicity assessment. Cells illumination was carried out at the bottom of the culture plates with orange light in sterile conditions [24] and cells were incubated again for additional 72 hours. The cell viability was then determined by the MTT

assay. Briefly, MTT was added to each well at the final concentration of 0.5 mg/mL in full medium and incubated at 37 °C with 5% $CO_2$ for 1h30. The medium was then removed, and the blue formazan product formed was dissolved in 200 µL DMSO. After 5 min shaking, the optical density (OD) at 570 nm of each well was measured using an ELISA plate reader (LT-5000 MS, Labtech). For each plate, each concentration was analyzed in triplicate.

**Analysis of PSs intracellular distribution with confocal laser scanning microscopy (CLSM)**

Cells (2 x $10^5$ cells) were deposited on 25 mm glass cover slips housed in 6-well plates and left to grow for 24h with 5% $CO_2$ at 37 °C. Cells were then incubated in full RPMI medium for 24h with the appropriate treatment (free PSs in DMSO or embedded into liposomes) and then rinsed with fresh full media. Prior to imaging, cells were incubated 15 min with 200 nM of MitoTracker® Green FM (ThermoFisher scientific, Invitrogen) in DPBS at 37 °C with 5% $CO_2$. After washing twice with DPBS, cells were incubated for 10 min with 10 µg/mL WGA Alexa Fluor 555 (ThermoFisher scientific, Invitrogen) in DPBS at 37°C with 5% $CO_2$. Cells were rinsed twice with DPBS, and cover slides were transferred to the confocal microscope chamber, supplemented with full culture medium. Samples were then imaged with an inverted Leica TCS SP8 microscope gated-STED (Leica, Germany) using a HC PL APO CS2 63x/1.40 oil immersion objective lens. The instrument was equipped with a 405 nm diode for porphyrin excitation, and a WLL Laser (490 nm excitation wavelength for MitoTrackerGreen and 555 nm for AlexaFluor 555). Far red, green and red fluorescence emission were collected respectively with a 650-800 nm, a 505-550 nm and a 560-630 nm wide emission slits under a sequential mode.

The statistical co-localization analysis of the photosensitizers with mitochondria and cell membrane was performed using ImageJ statistical plugin JACoP [30]. JACoP is a commonly used

tool for the calculation of colocalisation coefficient such as Manders' Co-localization Coefficient (MCC)[30] [31]. MCC was calculated for more than 20 cells.

## Results and discussion

### Synthesis of the lipid-porphyrin conjugates

Two lipid-porphyrin conjugates with different lipid backbones were synthesized (Scheme 1). One backbone was based on sn-1-palmitoyl lysophosphatidylcholine. This lipid was modified by the introduction of 6-(Fmoc-amino)hexanoic acid via direct acylation of the secondary alcohol groups at sn-2 position using sonication in the presence of glass beads, where the reaction is believed to take place. Such procedure aims to avoid intramolecular acyl migration as demonstrated previously by Rosseto *et al*.[31] and Oneill *et al*.[32]. Afterwards, the amino group was deprotected and followed by attachment of Pheo-a using HATU as coupling reagent to give PhLPC (compound 2, yield 65%).

The second lipid backbone, which is based on a Lyso-eSM was prepared by acidic hydrolysis of egg sphingomyelin (N-hexadecanoyl-D-erythro-sphingosylphosphorylcholine) in anhydrous methanolic hydrogen chloride at 50 °C following the same procedure as Bitmman *et al.* [33]. The mild acidic hydrolysis allowed the preparation of Lyso-eSM with low extent of C-3 epimerization compared to the conventional hydrolysis methods. The Pheo-a was then coupled via peptidic coupling using the same procedure as for PhLPC, to yield compound 4 (PhLSM, yield 30%).

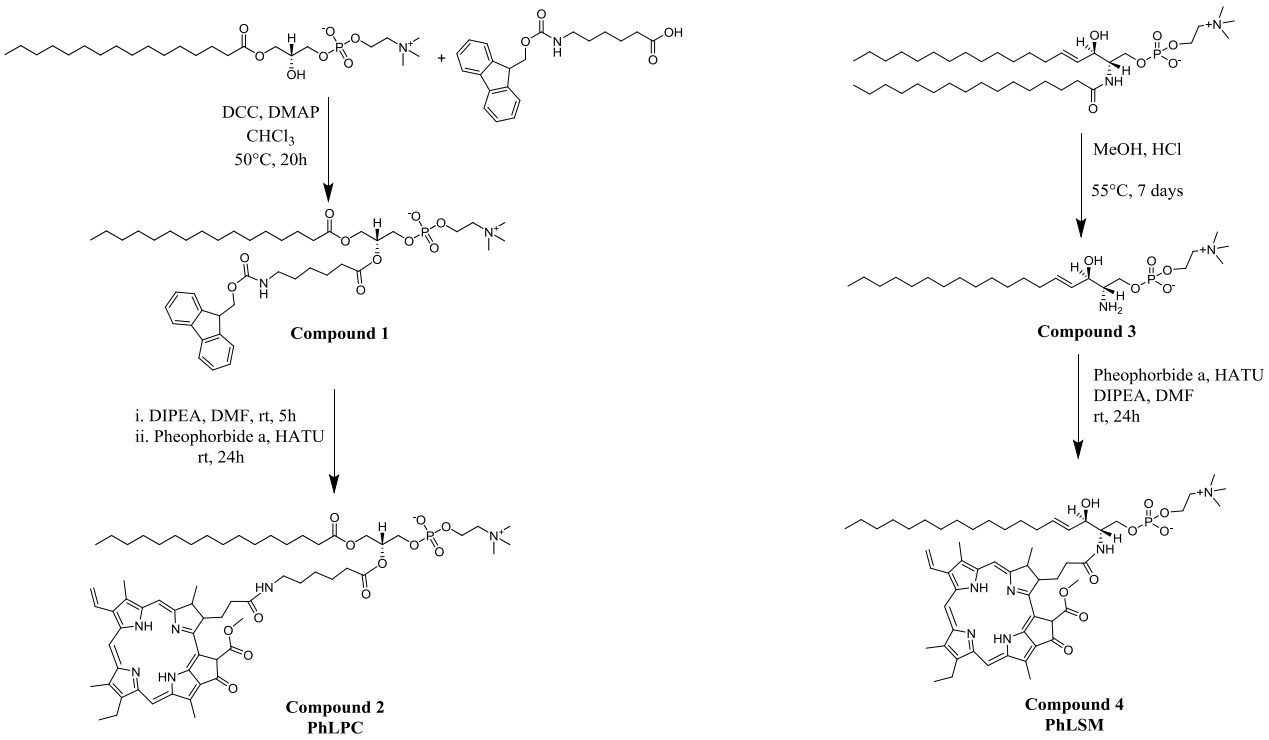


**Scheme 1.** Synthesis route for the porphyrin-lipid conjugates PhLPC (A) and PhLSM (B)

## Characterization of the self-assembling and photophysical properties of the lipid-porphyrin conjugates:

The ability of the synthesized compounds to self-assemble into organized structures similar to those reported for porphysomes was assessed after hydration of films made of PhLPC or PhLSM. The extruded suspensions were then analyzed by dynamic light scattering (DLS) and cryo-electron microscopy (Cryo-TEM). Interestingly, these suspensions were monodisperse (PdI < 0.2) and exhibited an average size of approximately 200 nm (Figure S5). Cryo-TEM micrographs revealed that both lipid-porphyrin conjugates could self-assemble into liposome-like structures with a dense bilayer of lipid-porphyrin conjugates surrounding an aqueous core (Fig 1C-D). The thickness of the bilayers was approximately 4-5 nm for both compounds, similar to that of

ordinary phospholipid bilayers [34]. However, whereas self-assembled PhLPC showed spherical shape, PhLSM ones exhibited ovoid shape with undulated bilayer. The impact of PhLPC and PhLSM vesicles on their photophysical properties was studied by recording their absorption and fluorescence spectra before and after their solubilization in HEPES buffer/methanol/THF (0.2 : 0.8 : 1 mL) mixture. (Fig. 1 E-H)

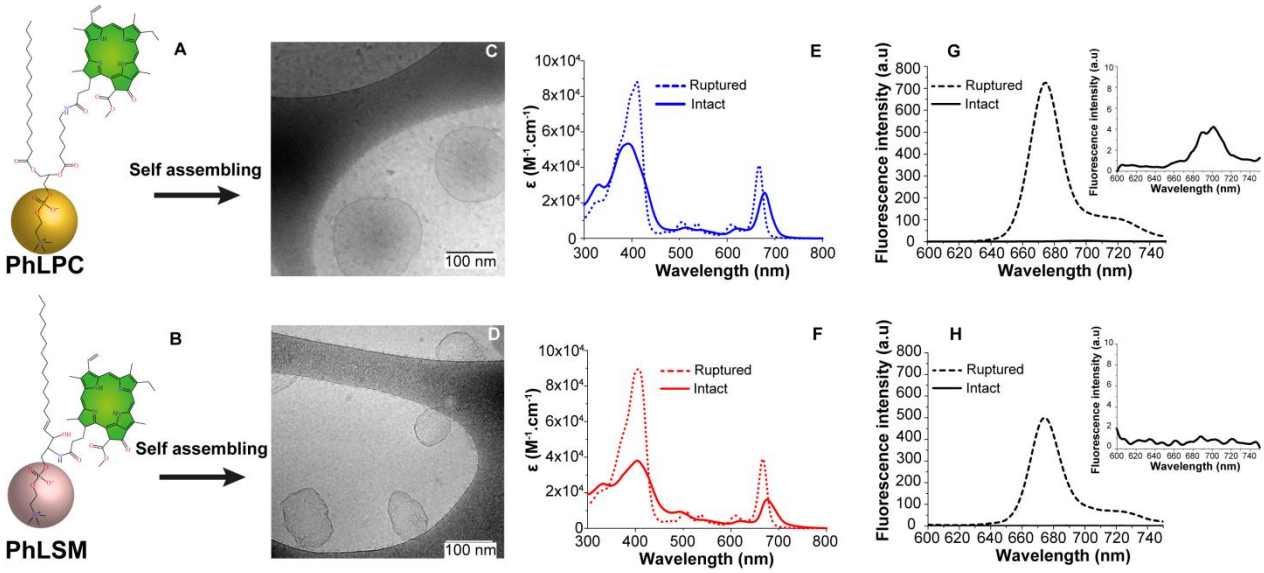


**Fig. 1** Schematic representation of (A) PhLPC and (B) PhLSM. Cryo-electron micrographs of self-assemblies made of pure (C) PhLPC and (D) PhLSM in HEPES buffer. Absorbance and fluorescence spectra of PhLPC (E, G) and PhLSM (F, H) vesicles, respectively before (solid line) and after (dashed line) their solubilization in HEPES/MeOH/THF (0.2, 0.8, 1 mL) mixture. The insets in (G) and (H) correspond to the quenched fluorescence spectra of PhLPC and PhLSM in buffer respectively.

As shown in Figure 1 and table 1, lipid-porphyrin conjugates exhibited similar absorption and fluorescence spectra to that of Pheo-a in organic solvents (Figure S6). This result indicates that linking Pheo-a to the lipid backbones did not induce any change in the photophysical properties of the PS when the PS-lipid conjugates were in their monomeric state. Conversely, nanoassemblies of both compounds showed several interesting features. First, absorption spectra

of both lipid-porphyrin vesicles revealed a broadening of porphyrin Soret and $Q_{max}$-bands with a significant red shift of approximately 12 nm for the latter. Compared to pure Pheo-a aggregates in buffer (Fig. S6), the Soret and $Q_{max}$-band of the lipid-porphyrin vesicles were sharper, indicating that they formed more organized aggregates within their vesicular structure. The extent of the intermolecular interaction between lipid-porphyrin conjugates within the dense bilayers of the lipid-porphyrin vesicles were further analyzed by investigating their fluorescence quenching. As shown in the insets to figures 1G and 1H, the fluorescence spectra of the vesicles were extensively quenched, compared to the corresponding monomers. Interestingly, the full fluorescence intensity of lipid-porphyrin conjugates could be efficiently restored with approximately 1000-fold intensity increase, after solubilization of the lipid-porphyrin conjugates in organic solvent. Similar behavior has been described by Lovell *et al.*[19b] for nanoassemblies made of pyro-lipids (pyropheophorbide-a linked to Lyso-PC via ester bond) that could be used as efficient photothermal and photoacoustic agents for tumor thermal ablation and photoacoustic imaging [19b]. Taken together, the strong quenching of fluorescence emission and the red shifted absorption of the studied compounds are proof of the strong intermolecular interactions existing between chromophores within the lipid-porphyrin vesicles. However, despite these interesting properties, these vesicles were not stable and formed larger aggregates of undefined structure within few days (Figure S7). These results are in line with those obtained by Zheng's group [19b, 20] with pyro-lipids assemblies to which addition of DSPC, cholesterol and DSPE-PEG was necessary to retain efficiently an encapsulated hydrophilic cargo, and to promote higher stability of the vesicles [19b, 20, 35]. In fact, the bilayer instability of the lipid-porphyrin conjugates can be due to the mismatch between the length of the alkyl chain in sn-1 position and the adjacent porphyrin, leading to an inadequate packing parameter for bilayer stability. The packing parameter, defined as $P = v/al$, where $v$ is the hydrocarbon chain volume, $a$ is the area of the

polar headgroup and *l* the length of the hydrocarbon chain [36], is useful to determine the preferential organization of a surfactant at high concentration in a liquid medium. Phospholipids form bilayers because their *P* value usually lies between 0.5 and 1 [36]. In the case of PhLSM, the porphyrin is grafted in the vicinity of the polar headgroup thus increasing its polar group area, and subsequently decreasing P to a value lower than 0.5 (conical or truncated conical shape). Conversely for PhLPC, the porphyrin is conjugated to the hydrophobic chain in sn-2, which may induce an increase in the hydrophobic volume leading to a *P* value higher than 1 (inverted conical shape) [37]. It has also been shown that when lipid molecules with complementary shapes are associated together, the value of *P* becomes additive resulting in the formation of intermediate blocks that can form a stable bilayer [37]. So, since the two studied lipid-porphyrin conjugates cannot form stable bilayers on their own, they could be mixed with unmodified phospholipids to counterbalance the effect of the length mismatch between alkyl chains.

| **Monomers** | | | |
|---|---|---|---|
| **Compounds** | **Pheo-a** | **PhLPC** | **PhLSM** |
| $\lambda_{max}$ **(Soret) [nm]** | 411 | 410 | 406 |
| $\varepsilon_{soret}$ **[$M^{-1}.cm^{-1}$]** | $9.9 \times 10^4$ | $8.8 \times 10^4$ | $8.9 \times 10^4$ |
| $\lambda_{max}$ **(Q) [nm]** | 667 (21) | 667 (20) | 667 (21) |
| $\varepsilon_Q$ **[$M^{-1}.cm^{-1}$]** | $3.4 \times 10^4$ | $4.1 \times 10^4$ | $3.9 \times 10^4$ |
| **Vesicles or aggregates** | | | |
| $\lambda_{max}$ **(Soret) [nm]** | 386 | 392 | 404 |
| $\varepsilon_{soret}$ **[$M^{-1}.cm^{-1}$]** | $3.1 \times 10^4$ | $5.3 \times 10^4$ | $3.8 \times 10^4$ |
| $\lambda_{max}$ **(Q) [nm]** | 674 (39) | 679 (30) | 676 (33) |
| $\varepsilon_Q$ **[$M^{-1}.cm^{-1}$]** | $0.7 \times 10^4$ | $2.5 \times 10^4$ | $1.6 \times 10^4$ |

**Table 1:** Soret band, Q-band and the corresponding absorption coefficient (**ε)** of monomeric (after vesicles solubilization in HEPES buffer/methanol/THF (0.2 : 0.8 : 1 mL) mixture) and aggregated forms (in HEPES buffer) of Pheo-a, PhLPC and PhLSM respectively. Values in brackets are the bandwidths (nm) at half height.

### Interfacial behavior of lipid-porphyrin conjugates

To further investigate the effect of the organization of the lipid-porphyrin conjugates on their self-assembling properties, we studied the interfacial behavior of the two compounds at the air-

buffer interface using a Langmuir trough. The π-A isotherms for Pheo-a and the lipid-porphyrin conjugates (PhLPC and PhLSM) spread at the air-buffer interface are shown in figure 2 A and the main characteristics are summarized in table 2. The data show that the three compounds formed stable monolayers and reveal interesting differences between them. The influence of the attachment of Pheo-a to the lyso-eSM backbone or to the sn-2 aliphatic chain of lyso-PC is readily apparent on the graph, showing significant differences in isotherm shape, surface pressure and molecular area at collapse between compounds. The surface pressure corresponding to the lateral pressure in membranes or phospholipid vesicles is close to 30 mN/m [38]. At this surface pressure, the molecular area of Pheo-a ($A_{30}$) was 53 $Å^2$. Considering the approximate dimensions of Pheo-a as determined using the Visual Molecular Dynamics (VMD) software [39], the experimental interfacial molecular area of the PS was much smaller than that expected for a Pheo-a molecule lying flat on the surface (~ 156 $Å^2$). Conversely, the experimental $A_{30}$ value for Pheo-a was in good agreement with the calculated value of the surface area of a Pheo-a molecule with carboxylic and ester groups facing the air/water interface (~ 55 $Å^2$). This arrangement would result from the formation of closely packed films of Pheo-a molecules, controlled by strong attractive π-π interactions between the rings of neighboring molecules.

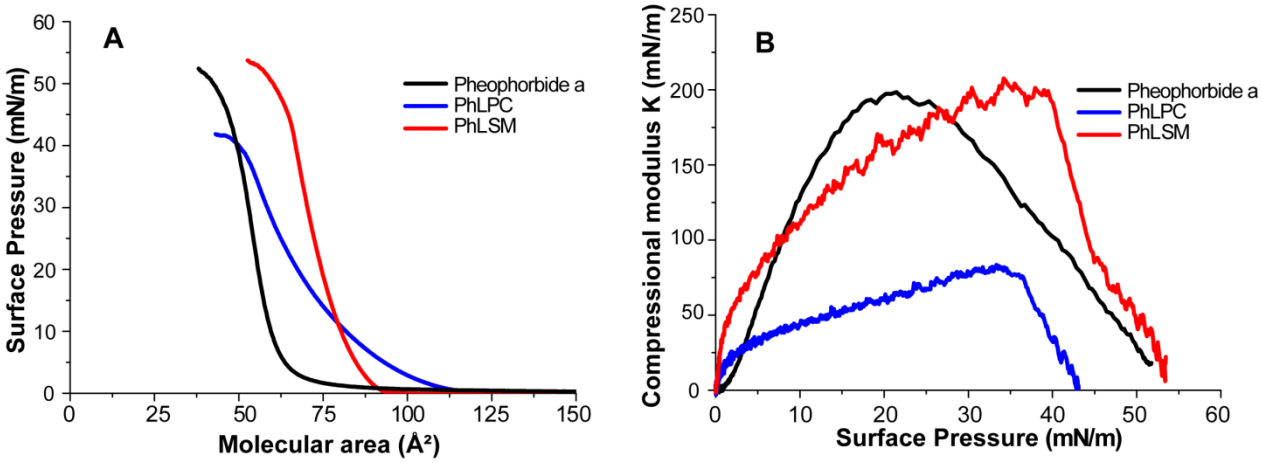

**Figure 2.** (A) π-A isotherms and the corresponding (B) compressional modulus for pure Pheo-a, PhLPC, and PhLSM spread at the air-buffer interface.

Both lipid-porphyrin conjugates formed more expanded monolayers with larger molecular areas at the surface pressure onset ($A_0$) for PhLPC (116 $Å^2$) and PhLSM (94 $Å^2$) compared to Pheo-a (80 $Å^2$). Surprisingly, while the molecular area expansion for PhLSM was maintained even at higher surface pressure, that of PhLPC at 30 mN/m was significantly reduced as compared to pure Pheo-a. In addition, while Pheo-a and PhLSM showed similar collapse surface pressure and similar π-A isotherms profile, PhLPC exhibited a completely different isotherm profile, with dissimilar shape, surface pressure and molecular area from those of the two other compounds.

Such behavior could be explained by different molecular arrangements of the studied molecules at the air/buffer interface. Apparently, grafting Pheo-a to the lyso-SM backbone did not affect its interfacial arrangement at the air/water interface and the area expansion of its isotherm could be only explained by the presence of the PC headgroup in the vicinity of the chromophore. However, the longer C6 carbon chain linker of PhLPC, bearing the Pheo-a at its extremity would provide more flexibility to the attached chromophore to adopt distinct local orientation at different surface pressure. Indeed, the onset of the surface pressure for the PhLPC is observed at a larger molecular area ( ~116 $Å^2$) than the other compounds due to the presence of the acyl chain bearing Pheo-a at the interface. Upon further monolayer compression, the molecular area of PhLPC decreased significantly to reach a collapse molecular area of ~50 $Å^2$ which lies between that of Pheo-a and PhLSM. However, it should be noticed that this molecular area is smaller than that of monounsaturated phospholipids ($A_c$ ~ 60-70 $Å^2$). Such behavior could be explained by the reorientation of the Pheo-a to align with the sn-1 C16 carbon chain with subsequent solubilization of molecules into the subphase during the compression. To gain further insight into the structural

characteristics of the lipid-porphyrin conjugates, the compressibility moduli of their isotherms were calculated and plotted as a function of surface pressure. As shown in Figure 2B and Table 2, a similar compressional modulus range is revealed for Pheo-a and PhLSM with a $K_{max}$ value approaching ~ 200 mN/m. However, PhLPC exhibits a much lower value (~ 80 mN/m). According to Davies and Rideal [40], the values of PhLSM and Pheo-a would correspond to the liquid condensed state (100 mN/m < $K_{max}$ < 250 mN/m), while that of PhLPC would indicate a monolayer in liquid-expanded state ($K_{max}$ < 100 mN/m). Thus, PhLPC formed a less organized monolayer than the other studied compounds.

| **Monolayer composition** | **$A_0$ (Å$^2$)** | **$A_{30}$ (Å$^2$) at 30 mN/m** | **$A_c$ (Å$^2$)** | **$\pi_c$ (mN/m)** | **$K_{max}$ (mN/m)** |
|---|---|---|---|---|---|
| **Pheo-a** | 80 | 53 | 41 | 50.2 | 198.5 |
| **PhLPC** | 116 | 60 | 50 | 41.5 | 82.6 |
| **PhLSM** | 94 | 72 | 64 | 51.5 | 205.4 |

**Table 2:** Molecular area at surface pressure onset ($A_0$), molecular Area ($A_{30}$) at surface pressure of 30 mN/m, molecular Area (Ac), surface Pressure ($\pi_c$) at collapse, and maximal compressional modulus $K_{max}$ for compounds monolayers.

**Analysis of the fine structures of Pheo-a derivatives monolayers**

To get a better understanding of the fine structures perpendicular to the plane of Pheo-a derivatives monolayers, the specular X-ray reflectivity (XRR) was measured on monolayers compressed to a surface pressure of 30 mN/m. Figure 3A, shows the XRR curves of Pheo-a, PhLPC and PhLSM monolayers spread on HEPES buffer, fitted using a two-slab model. The corresponding electron density profiles ($\rho$) reconstructed from the best fit results (solid red lines in figure 3A) along the z-axis are also shown in figure 3B. The thickness (d), electron density ($\rho$)

and root mean square roughness ($\sigma$) of each interface are summarized in table 3. Pheo-a exhibited total thickness $d_{pheo-a}$ of 15.7 Å. The hydrophobic core had a thickness of 9.5 Å and an electron density of 0.436 $e^- \times Å^{-3}$. Since these values are consistent with those reported for other porphyrin monolayers [41], it is plausible that Pheo-a molecules take an upright orientation with respect to the interface (Figure 3C). In fact, this result agrees well with the area per molecule and compression modulus determined from π-A isotherms (Figure 2). The thickness and electron density of the hydrophobic regions of the PhLPC monolayer are $d_{HC(PHLPC)}$ 11.6 Å and $\rho_{HC(PhLPC)}$ = 0.373 e- × Å−3 , respectively. Interestingly, the corresponding values for the PhLSM monolayer are $d_{HC(PHLSM)}$ 9.4 Å and $\rho_{HC(PhLSM)}$ of 0.391 $e^- \times Å^{-3}$, respectively. The $\rho_{HC}$ values of both compounds are higher than those reported for saturated [42] or monounsaturated [43] alkyl chains of phospholipids. This could suggest the presence of porphyrin core within the alkyl chains. Although the thickness of hydrophobic region of PhLPC is larger than that of PhLSM, it is notable that the total thickness of PhLPC ($d_{PhLPC}$ = 21.5 Å) is 2 Å thicker than that of PhLSM ($d_{PhLSM}$ = 19.5 Å). This could be explained in terms of the conformational difference of the porphyrin. In the case of PhLPC, sn-1 C16 carbon chain and porphyrins are aligned (Figure 3C, middle) while such an alignement is sterically prohibited in the case of PhLSM. In order to validate the fitting quality, the average number of electrons per molecule was calculated from the fit and compared to that calculated from the chemical formula of the studied compounds. As shown in table 3, there is a good agreement between the calculated number of electrons and the theoretical one for Pheo-a and PhLSM. Conversely for PhLPC, there is a significant difference between the number of electrons calculated from the molecular formula and that from the fit. This discrepancy could be interpreted by the error in PhLPC molecular area evaluation, due to its solubilization into buffer subphase.

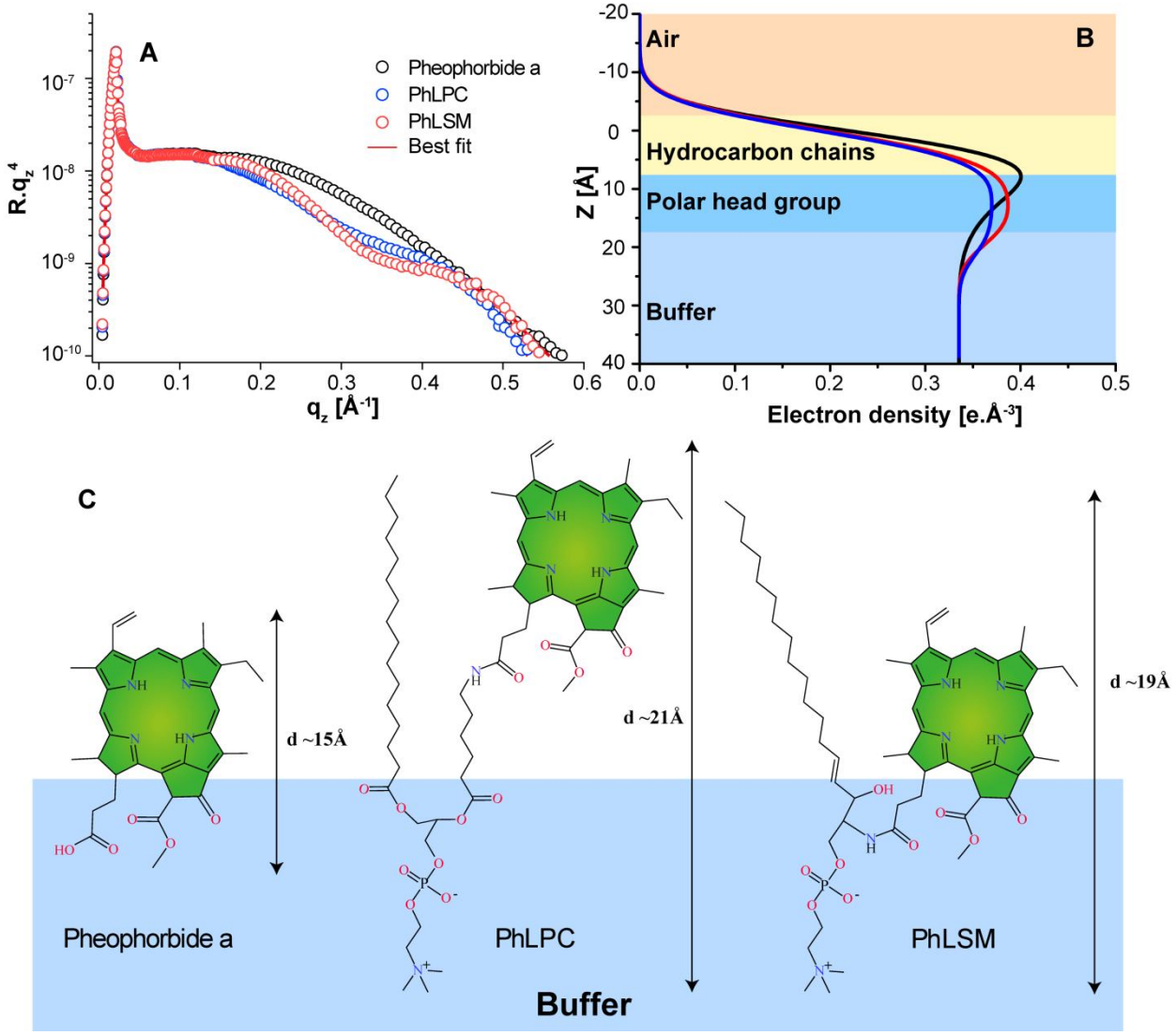


**Figure 3:** (A) XRR curves of a Pheo-a derivatives monolayers at a surface pressure of 30 mN/m. The solid lines represent the best model fits to the experimental data. The experimental errors are within the symbol size. (B) The reconstructed electron density profiles along the Z-axis. (C) Schematic representation of the orientation of pheo-a derivatives at the air/buffer interface.

| | d (Å) | ρ ($e^- \times Å^{-3}$) | σ (Å) | Average number of $e^-$/molecule from the fit | Theoretical number of $e^-$/molecule |
|---|---|---|---|---|---|
| **Pheophorbide-a** | | | | | |
| **Hydrophobic core** | 9.5 ± 0.3 | 0.436 ± 0.007 | 4.1 ± 0.1 | 342 | 314 |
| **Hydrophilic groups** | 6.2 ± 0.5 | 0.372 ± 0.010 | 4.1 ± 0.5 | | |
| **Buffer** | ∞ | 0.335 | 4.5 ± 0.6 | | |
| **PhLPC** | | | | | |
| **Hydrophobic chains** | 11.6 ± 0.5 | 0.373 ± 0.001 | 4.4 ± 0.8 | 462 | 638 |
| **Choline headgroup** | 9.8 ± 0.5 | 0.369 ± 0.001 | 3.6 ± 0.5 | | |
| **Buffer** | ∞ | 0.335 | 3.1 ± 0.1 | | |
| **PhLSM** | | | | | |
| **Hydrophobic chains** | 9.4 ± 0.6 | 0.391 ± 0.001 | 4.3 ± 0.1 | 546 | 560 |
| **Choline headgroup** | 10.1 ± 0.6 | 0.387 ± 0.001 | 4.6 ± 0.8 | | |
| **Buffer** | ∞ | 0.335 | 3.1 ± 0.1 | | |

**Table 3: Best fit parameters for the XRR Results for Pheo-a derivatives monolayers at 30mN/m as presented in Figure 3.**

## Miscibility of Pheo-a derivatives with phospholipids

We then evaluated the behavior of porphyrin derivatives when mixed with lipids in order to determine if these compounds could form stable systems when incorporated in a liposomal bilayer. To do so, we chose DSPC as phospholipid, and mixed it with increasing molar percentage of lipid-porphyrin derivatives. The recorded π-A isotherms of pure DSPC and its mixture with Pheo-a, PhLPC and PhLSM at the air/buffer interface are shown in Fig. 4 A, B and C, respectively. Pure DSPC formed a condensed phase as previously reported [44].

DSPC/Pheo-a mixtures did not behave in the same manner when the molar percentage of Pheo-a increased. Indeed, the isotherms for mixtures containing up to 10 mol% Pheo-a were shifted toward larger molecular areas than that of pure DSPC, but remained still in between the isotherms of the pure components up to 30 mN/m. However, at higher surface pressures, the isotherms of DSPC/Pheo-a exhibited slight shoulders at approximately 33 mN/m, 40 mN/m and 44 mN/m for monolayers containing 2.5%, 5% and 10% of Pheo-a respectively. This behavior could be related to the solubilization of some Pheo-a in the aqueous phase. Interestingly, the isotherms for the mixtures with a Pheo-a content higher than 10% were shifted toward larger

molecular areas than that of the pure Pheo-a indicating unfavorable interactions between the two components. A similar behavior was observed for mixed DSPC/PhLSM monolayers. However, unlike DSPC/Pheo-a mixtures, the isotherms for DSPC/PhLSM monolayers exhibited shoulders at higher surface pressure (around 40 mN/m). Furthermore, the isotherms were all intercalated between those of the pure components, even at 50 mol% PhLSM, which would account for a better miscibility of DSPC with PhLSM than with the free Pheo-a.

The compression isotherms of DSPC-PhLPC mixtures exhibited sharp inflection followed by a plateau region at ~ 43 mN/m. This sharp inflection is observed at a surface pressure close to that of pure PhLPC collapse and lower than that of pure DSPC. This could be interpreted as a demixing between the two compounds, with subsequent loss of PhLPC from the monolayer in the aqueous subphase. Similar behavior has been observed by Kinnunen's group who demonstrated that addition of oxidized phospholipids to phospholipid monolayers induced phase separation and their solubilisation in the subphase, with subsequent micelles formation due to the presence of polar groups (either carbonyl or carboxylate) on the sn-2 chain [45]. In the case of PhLPC, the driving force for the phase separation would be due to the strong attractive π-π interaction between Pheo-a cores.

The isotherms of the mixtures were further analyzed in terms of compressibility modulus as shown in Figures 4 D-F. In fact, for the three mixtures, adding a porphyrin or a porphyrin derivative to a DSPC monolayer induced a decrease in their rigidity with a more significant decrease in the presence of PhLPC, as expected from the low surface compressional modulus of this conjugate. In addition, compared to DSPC/Pheo-a mixtures, the sharp inflection point observed for the isotherms of PhLPC mixtures at high surface pressure (~ 40mN/m) is clearly revealed by a minimum in K at ~ 44 mN/m, close to the $\pi_c$ of pure PhLPC, followed by an

increase until the K values superimpose with those of pure DSPC. This is another indication of the complete expulsion of PhLPC from the monolayers at high surface pressure. In order to analyze quantitatively the thermodynamics of interaction between the binary mixtures, the excess free energy of mixing ($\Delta G^{Exc}$) was calculated up to a surface pressure of 30 mN/m. As inferred from Figures 4G-I, the $\Delta G^{Exc}$ values of binary mixtures of DSPC-Pheo-a and DSPC-PhLPC at different surface pressures are positive for the various PS molar fractions denoting repulsive interactions between DSPC and PS compounds in the mixtures. However, the situation is different for DSPC-PhLSM mixture. Indeed, this latter exhibited positive $\Delta G^{Exc}$ values up to 10% PhLSM, which then decreased down to values close to 0 at 50%. In addition, it should be stressed that $\Delta G^{Exc}$ values were the highest for DSPC-Pheo-a followed by DSPC-PhLPC and DSPC-PhLSM, thus indicating that interactions in the mixed films containing lipid-porphyrin conjugates were less repulsive than those in monolayers containing Pheo-a. Taken together, these results indicate that the three Pheo-a derivatives cannot be homogeneously mixed with DSPC and tend to segregate in the lipid monolayer.

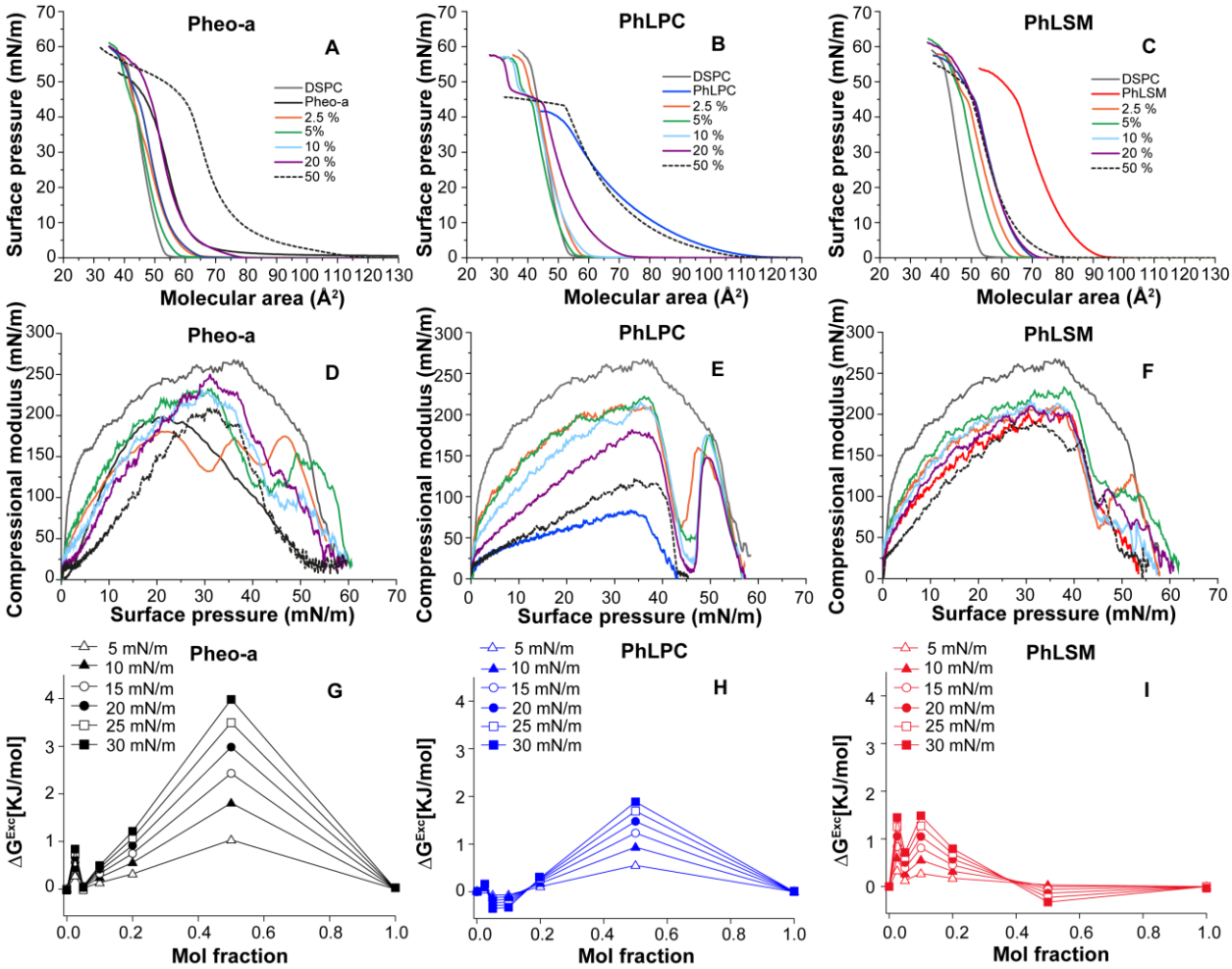


**Figure 4.** π-A isotherms of mixed monolayers of Pheo-a (A), PhLPC (B) and PhLSM (C) with DSPC at various molar %. Their corresponding compressional modulus and excess free energy of mixing ($\Delta G^{exc}$) are shown in (D-F) and (G-I) respectively.

## The incorporation of lipid-porphyrin conjugates into liposomes

In a next step, we investigated the incorporation efficiency of Pheo-a derivatives into liposomes, and evaluated their impact on their stability. DSPC liposomes doped with 2.5 mol% of DSPE-$PEG_{2000}$ and increasing molar percentages (2.5-20 mol %) of Pheo-a derivatives were prepared and characterized. As shown in figure S8, the highest Pheo-a loading rate was 5 mol%, but the liposomes increased in diameter and polydispersity. An important loss of material was also observed on the polycarbonate membrane during extrusion (Figure S8). A higher loading efficiency was achieved with PhLPC and PhLSM, with monodisperse vesicle suspensions and no significant material loss during extrusion.

We measured the fluorescence of DSPC liposomes incorporating the different PSs at 2.5 mol %. As depicted in Figure S9, the three PSs showed fluorescence quenching. The highest values were obtained for PhLSM and PhLPC. Such fluorescence quenching could be explained by the aggregation of the PSs into organized patterns in the bilayer due to their high packing density. Similar behavior has been observed by Gang Zheng's group with other lipid-porphyrin conjugates when incorporated within liposomal bilayers, and it was attributed to the formation of J-aggregates [46].

**Thermotropic behavior of phospholipid bilayers incorporating lipid-porphyrin conjugates**

PS aggregation in the membrane of liposomes could be an issue for liposomal delivery of photosensitizing agents for PDT applications. Indeed, the aggregation of PSs such as Pheo-a induces a decrease in the quantum yield of triplet state ( $\Phi_t$), thus reducing the quantum yield of singlet oxygen ($^1O_2$) [11, 47], which is responsible for the photodynamic activity. Therefore, in order to investigate the impact of the PSs incorporation percentage on their oxidative potential upon illumination, we performed a calorimetric analysis of SOPC lamellar suspensions incorporating different molar percentage of either PhLSM or PhLPC. SOPC was chosen in these experiments because it contains an unsaturated alkyl chain that is a good substrate for the formation of lipid hydroperoxides [24] upon interaction with singlet oxygen during the photodynamic reaction. The formation of such species can induce a phase separation within the lipid matrix that can be easily detected by DSC. Although qualitative, such method allows the determination of the optimal molar percentage of embedded PSs for efficient photodynamic activity.

First, the impact of PSs incorporation percentage on the phase behavior of the SOPC membrane was assessed. Fig. 5 shows the heat capacity ($C_p$) scans for the various lamellar suspensions. Compared to pure SOPC which exhibited a sharp endothermic peak at ~6 °C, both conjugates caused a broadening of the main transition peak and a shift toward lower temperatures in a concentration-dependent manner. This suggested the destabilization of the intermolecular cooperativity of SOPC molecules. Such tendency was more pronounced for PhLSM, which could be explained by its higher disordering effect on the hydrocarbon chains of phospholipids and/or its higher incorporation efficiency than that of PhLPC.

DSC scans were also performed after illumination of the SOPC lamellar suspensions in the conditions described in the experimental section. Compared to the pure SOPC sample, the illumination of samples containing up to 2.5 mol % of either PhLPC or PhLSM induced dramatic changes in the thermograms. The main transition peaks of both SOPC-PhLPC and SOPC-PhLSM samples were broadened with a significant shift of $T_{onset}$ towards lower temperatures and the appearance of a second peak/shoulder at lower temperature. These results indicate the formation of new phases upon illumination of the SOPC–PS systems, which could be related to the formation of new chemical species within the lipid bilayer, as demonstrated in our previous work [24]. It should be noticed, however, that the impact of the illumination was more pronounced in PhLPC samples than in those of PhLSM. This could be explained by the longer spacer of PhLPC compared to PhLSM, which would allow the Pheo-a moiety to be more deeply inserted into the lipid bilayer. Hence, the singlet oxygen generated upon illumination would have greater probability to oxidize the unsaturated chains within the lipid matrix.

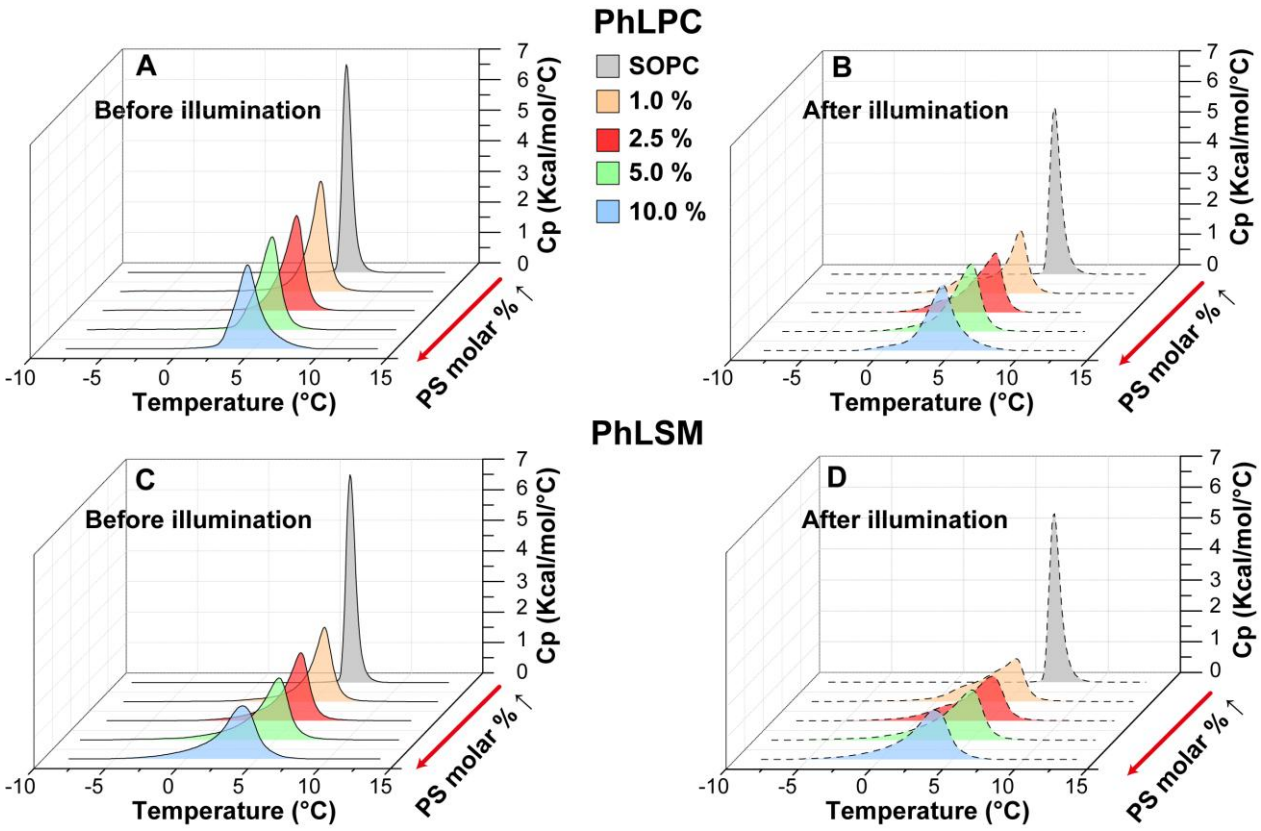


**Figure 5.** DSC heating scans for pure SOPC lamellar suspensions incorporating increasing molar percentages of PhLPC or PhLSM before (A,C) and after (B,D) illumination.

The illumination of samples containing more than 2.5% mol of PSs did not induce a significant change (Figure, 5, Table S1-2) in their thermal behavior, which could be due to PS aggregation in the lipid membranes. Based on the aforementioned, we formulated liposomes with only 2.5% mol of PS and their photodynamic efficiency was then evaluated *in vitro* on esophageal cell lines.

**Phototoxicity of lipid-porphyrin conjugates in esophageal squamous cell carcinoma (ESCC) cell lines**

The phototoxicity of Pheo-a derivatives (Pheo-a, PhLPC and PhLSM), free or incorporated in DSPC/DSPE-$PEG_{2000}$ liposomes (95/2.5 mol%), was investigated on Kyse-30 and HET-1A cells. After overnight incubation with either free or incorporated PSs, the cells were illuminated for 14

min, and the phototoxicity of the three compounds was quantified by the MTT test (Fig. 6). The cytotoxicity in darkness was found to be negligible with a survival percentage close to 100% for the three PSs in the 0.1-5 µM concentration range (figure S10). As shown in Figure 6, free or liposomal Pheo-a exhibited a strong phototoxicity on both cell lines with a half maximal inhibitory concentration (IC50) of 0.20 and 0.15 µM, respectively (Figure 6, table S4). These IC50 values for Pheo-a are in agreement with those previously reported by Rapozzi *et al.* [48] for other cancer cell lines.

The IC50 of the lipid-porphyrin conjugates was in all cases significantly higher than that of Pheo-a, thus indicating a decrease in Pheo-a phototoxic activity when in the form of lipid conjugates (table S4). This behavior could be related to lipid-porphyrin conjugate aggregation in aqueous media, which in turn would reduce their photodynamic activity.

The same explanation could be applied to these compounds when incorporated in liposome bilayers. Indeed, although the Pheo-a conjugates incorporated in liposomes maintained their photoactivity at this percentage of incorporation, as demonstrated by DSC experiments, the fluorescence intensity of embedded conjugates was partially quenched, and this effect was higher than with Pheo-a (Figure S9). This fluorescence quenching is explained by the aggregation of Pheo-a conjugates within the lipid bilayer because of π- π stacking of porphyrin cores. This in turn would cause a decrease in the quantum yield of the singlet oxygen and thus, a decrease in the photodynamic efficiency of lipid-porphyrin conjugates as compared to Pheo-a incorporated in liposomes.

However, it should be noted that despite this decrease in phototoxicity for both lipid-porphyrin conjugates compared to Pheo-a, they can still be considered as strong photosensitizers with IC50 values between 1 and 2 µM for the cancerous Kyse-30 cell line. Interestingly, PhLPC and PhLSM exhibited a selective phototoxicity toward this cell line, especially when incubated with

the cells in their free form. Indeed, whereas the IC50 of the free PhLPC and PhLSM were 1.4 µM and 2.1 µM in Kyse-30 cells, respectively, they were higher for HET-1A cells, with 2.5 µM and > 5µM respectively. This striking result could be explained by different cellular uptake and/or subcellular localization in cancerous cells compared to healthy ones. Indeed, several studies have shown that PSs internalization mechanism and subcellular localization are major determinants of their phototoxicity [10a, 49].

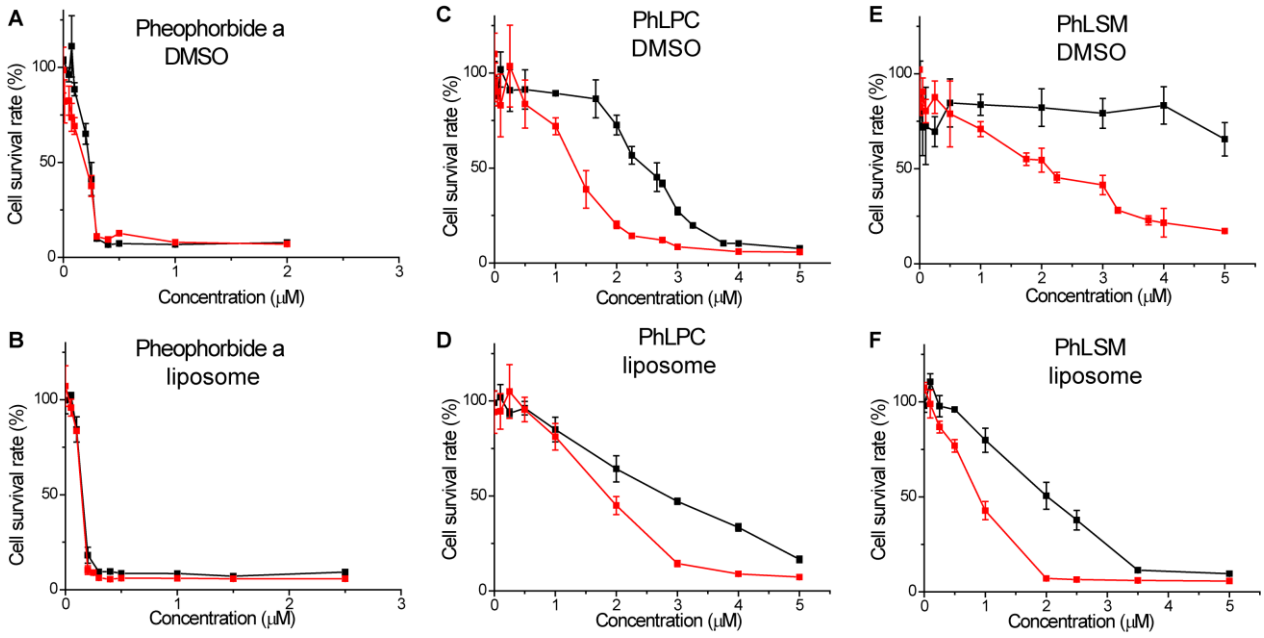


**Figure 6.** Phototoxicity HET-1A (black line) and Kyse-30 (red line) incubated with free pheophorbide a (A), PhLPC (C), or PhLSM (E), or encapsulated in liposomes (B, D, F respectively).

## Cellular uptake and subcellular localization

In order to evaluate the cellular uptake of the different PSs, as well as their subcellular distribution, we applied confocal laser scanning microscopy on HET-1A and Kyse-30 cells after overnight incubation with the studied PSs, either free or incorporated into DSPC liposomes. Figure 7 shows that the nucleus remained dark in all cases, and that the fluorescence signal of the

three PSs was mainly inside the cytoplasm, indicating their effective internalization. The fluorescence distribution of free Pheo-a dissolved in DMSO versus liposomal formulation revealed in both cases a broadly diffused fluorescence with no obvious difference between the two cell lines. In comparison with Pheo-a, the cellular distribution of fluorescence of free lipid-porphyrin conjugates was punctuated, which could be related to PSs localization into specific intracellular compartments such as mitochondria or lysosomes. Similar tendency was observed for lipid-porphyrin conjugates embedded into liposomes.

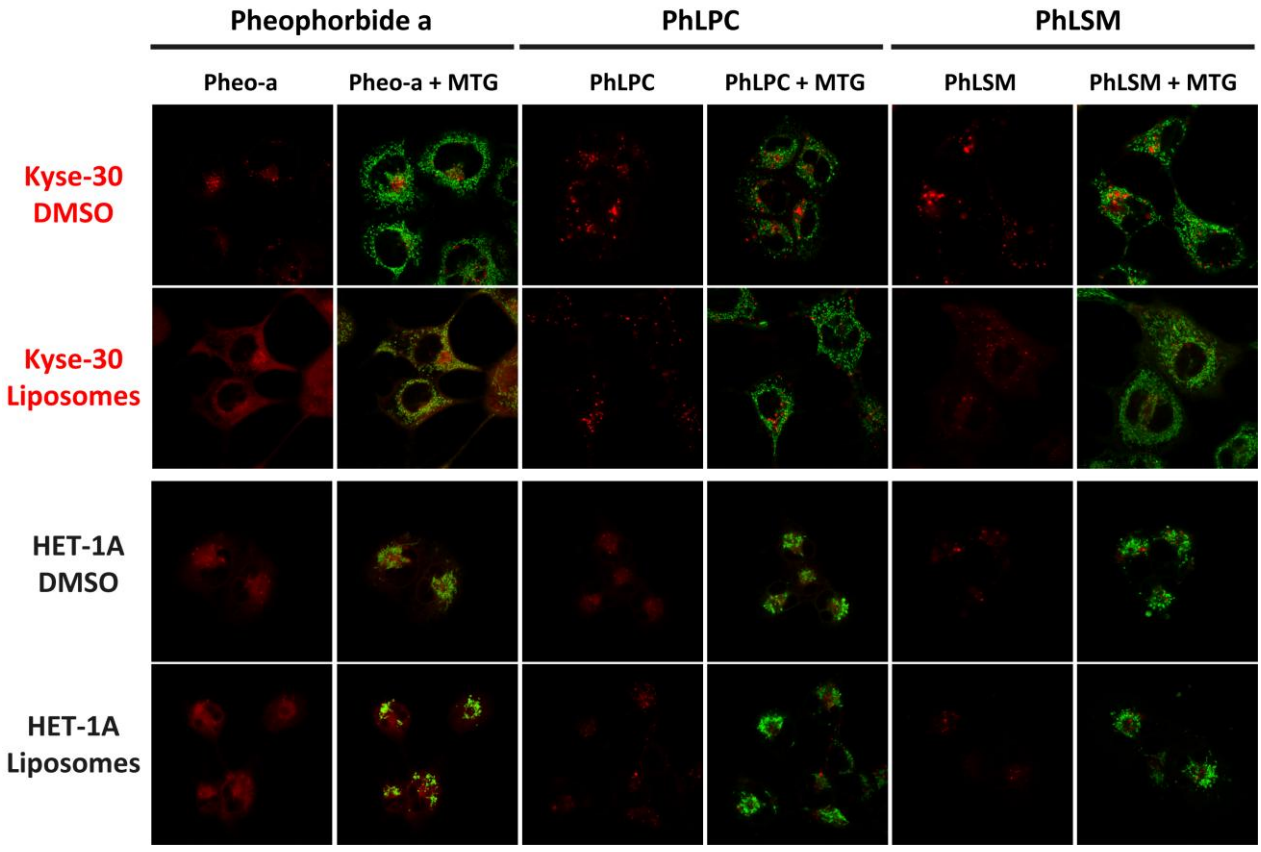


**Figure 7.** (a) Confocal microscopy images of Kyse-30 and HET-1A cells treated with the free photosensitizers (red) dissolved in DMSO or incorporated into liposomes. The second column for each compound corresponds to the images merged with those in the presence of Mitotracker (green).

Since the pure pheo-a and its derivatives may have higher affinity for mitochondria compared to other cell organelles [11, 48], we investigated the co-localisation of the PSs with mitochondria using Mitotracker-green. The images in Figure 7 and their statistical analysis performed using ImageJ statistical plugin JACoP and the Manders' coefficient of co-localization (MCC), show that Pheo-a exhibited higher MCC (0.41-0.50) than the lipid-Pheo-a conjugates in both cell lines, without significant difference between Kyse-30 and HET-1A cells (Table S5). This could explain the higher photoactive efficiency of Pheo-a compared to the conjugated molecules, but also its non-selectivity towards the cancerous cell line [50]. The Pheo-a conjugates exhibited the lowest MCC values for HET-1A cells. Moreover, the MCC evolution of Pheo-a conjugates in both cell lines with the different formulations seemed to correlate with their IC50 values. This result would indicate the preferential affinity of PhLPC and PhLSM for the mitochondria in the cancerous cell line.

# Conclusion

In this work, we have synthesized and characterized two new lipid-porphyrin conjugates which exhibit self-assembly properties. These molecules were designed in the aim to improve the photosensitizers loading efficiency in liposome bilayers, and enhance PS photodynamic activity against cancerous cells. The addition of the lipid backbone exacerbated the amphipathic character of the photosensitizer, while maintaining its photodynamic activity. Both conjugates were able to self-assemble in buffer, however they were unstable and formed aggregates with unclear structure within few days. Such instability could be related to mismatch between the length of the alkyl chain in sn-1 position and the adjacent porphyrin, which would affect the lipid packing parameter. Both lipid porphyrin conjugates could be incorporated efficiently in lipid vesicles,

with higher loading rates than Pheo-a. We determined the maximal molar ratio of the PS-conjugates for maintaining their photodynamic activity. The phototoxicity of free or incorporated lipid-porphyrin conjugates was studied in two esophageal squamous cell lines. Although less photoactive than free Pheo-a, both lipid-porphyrin conjugates exhibited higher selectivity towards the studied cancerous esophageal cell line. However, such behavior was investigated only on two esophageal cell lines, thus further *in vitro* and *in vivo* studies will be needed in the future in order to confirm the possible preferential tumor-localizing properties of Pheo-a conjugates.

Interestingly, lipid-porphyrin conjugates carried by liposomes exhibited high fluorescence quenching yields. This means that upon their illumination, the absorbed photon energy could be dissipated into heat. Thus, although their photodynamic efficiency (IC50) was lower than that of Pheo-a, their self-quenching property in lipid vesicles could be taken advantage of, for use as efficient cytotoxic photothermal agents (PTT). Moreover, such systems could be used for photo-triggered release of encapsulated chemotherapeutic agents. Although they were not explored in this work, these aspects deserve further investigations in the future. Hence, liposomes containing lipid-porphyrins conjugates would present a promising photoactivatable drug delivery system with multifunctional properties (PDT, PTT and photo-triggered release of an anticancerous drug) against cancer tumors.

# Acknowledgments

We thank ESRF for synchrotron beam time, Lukas Scheiderer for his experimental help and Dr. W. Abuillan for helpful discussion on XRR experiments. The authors are grateful to Camille Dejean (BioCIS, Châtenay-Malabry, France) for her help for NMR spectra analysis and the

fruitful discussions, to Dr Sylvain Trépout (Institut Curie,Orsay, France) for his contribution to cryoTEM experiments, to Stéphanie Denis for her technical assistance in cell culture and to Dr. Sylviane Lesieur (Institut Galien Paris-Sud) for discussion on DSC experiments. JM is thankful to the French Ministry of Research for the financial support of his PhD thesis.

# References

[1] L. R. Milgrom, *The Colours of Life: An Introduction to the Chemistry of Porphyrins and Related Compounds*, Oxford University Press, **1997**, p. 1-22.
[2] M. D. Daniell and J. S. Hill, *Aust N Z J Surg* **1991**, *61*, 340-348.
[3] T. J. Dougherty, C. J. Gomer, B. W. Henderson, G. Jori, D. Kessel, M. Korbelik, J. Moan and Q. Peng, *Journal of the National Cancer Institute* **1998**, *90*, 889-905.
[4] A. B. Ormond and H. S. Freeman, *Materials (Basel)* **2013**, *6*, 817-840.
[5] a) D. A. Bellnier, W. R. Greco, G. M. Loewen, H. Nava, A. R. Oseroff and T. J. Dougherty, *Lasers Surg Med* **2006**, *38*, 439-444; b) E. C. Halperin and C. A. Perez, *Perez and Brady's Principles and Practice of Radiation Oncology*, Wolters Kluwer/Lippincott Williams & Wilkins, **2013**, p.
[6] B. Tan Ing, G. Dolivet, P. Ceruse, V. Poorten Vincent, G. Roest and W. Rauschning, *Head & Neck* **2010**, *32*, 1597-1604.
[7] M. Kramer, J. W. Miller, N. Michaud, R. S. Moulton, T. Hasan, T. J. Flotte and E. S. Gragoudas, *Ophthalmology* **1996**, *103*, 427-438.
[8] Y. N. Konan, R. Gurny and E. Allémann, *Journal of Photochemistry and Photobiology B: Biology* **2002**, *66*, 89-106.
[9] M. Sadasivam, P. Avci, G. K. Gupta, S. Lakshmanan, R. Chandran, Y. Y. Huang, R. Kumar and M. R. Hamblin, *Eur J Nanomed* **2013**, *5,* 115–129.
[10] a) I. Laville, S. Pigaglio, J. C. Blais, F. Doz, B. Loock, P. Maillard, D. S. Grierson and J. Blais, *J Med Chem* **2006**, *49*, 2558-2567; b) S. Ballut, A. Makky, B. Chauvin, J. P. Michel, A. Kasselouri, P. Maillard and V. Rosilio, *Org Biomol Chem* **2012**, *10*, 4485-4495.
[11] V. Rapozzi, M. Zacchigna, S. Biffi, C. Garrovo, F. Cateni, M. Stebel, S. Zorzet, G. M. Bonora, S. Drioli and L. E. Xodo, *Cancer Biology & Therapy* **2010**, *10*, 471-482.
[12] a) J. Son, S. M. Yang, G. Yi, Y. J. Roh, H. Park, J. M. Park, M. G. Choi and H. Koo, *Biochem Biophys Res Commun* **2018**, *498*, 523-528; b) D. Zhang, M. Wu, Y. Zeng, L. Wu, Q. Wang, X. Han, X. Liu and J. Liu, *ACS Appl Mater Interfaces* **2015**, *7*, 8176-8187; c) M. A. Rajora, J. W. H. Lou and G. Zheng, *Chem Soc Rev* **2017**, *46*, 6433-6469.
[13] a) I. Roy, T. Y. Ohulchanskyy, H. E. Pudavar, E. J. Bergey, A. R. Oseroff, J. Morgan, T. J. Dougherty and P. N. Prasad, *J Am Chem Soc* **2003**, *125*, 7860-7865; b) K. Zaruba, J. Kralova, P. Rezanka, P. Pouckova, L. Veverkova and V. Kral, *Org Biomol Chem* **2010**, *8*, 3202-3206.
[14] a) G. Obaid, M. Broekgaarden, A. L. Bulin, H. C. Huang, J. Kuriakose, J. Liu and T. Hasan, *Nanoscale* **2016**, *8*, 12471-12503; b) X. Damoiseau, H. J. Schuitmaker, J. W. Lagerberg and M. Hoebeke, *J Photochem Photobiol B* **2001**, *60*, 50-60; c) M. J. Bovis, J. H. Woodhams, M. Loizidou, D. Scheglmann, S. G. Bown and A. J. Macrobert, *J Control Release* **2012**, *157*, 196-205; d) M. A. Rajora, L. Ding, M. Valic, W. Jiang, M. Overchuk, J. Chen and G. Zheng, *Chem Sci* **2017**, *8*, 5371-5384.

[15] a) V. J. Venditto and F. C. Szoka, Jr., *Adv Drug Deliv Rev* **2013**, *65*, 80-88; b) J. I. Hare, T. Lammers, M. B. Ashford, S. Puri, G. Storm and S. T. Barry, *Adv Drug Deliv Rev* **2017**, *108*, 25-38; c) J. C. Leroux, *Angew Chem Int Ed Engl* **2017**, *56*, 15170-15171.
[16] a) A. S. Derycke and P. A. de Witte, *Adv Drug Deliv Rev* **2004**, *56*, 17-30; b) B. Chen, B. W. Pogue and T. Hasan, *Expert Opin Drug Deliv* **2005**, *2*, 477-487.
[17] R. K. Jain, *J Control Release* **2001**, *74*, 7-25.
[18] B. Q. Spring, R. B. Sears, L. Z. Zheng, Z. M. Mai, R. Watanabe, M. E. Sherwood, D. A. Schoenfeld, B. W. Pogue, S. P. Pereira, E. Villa and T. Hasan, *Nature Nanotechnology* **2016**, *11*, 378-+.
[19] a) E. Huynh and G. Zheng, *Nano Today* **2014**, *9*, 212-222; b) J. F. Lovell, C. S. Jin, E. Huynh, H. Jin, C. Kim, J. L. Rubinstein, W. C. Chan, W. Cao, L. V. Wang and G. Zheng, *Nat Mater* **2011**, *10*, 324-332.
[20] K. A. Carter, S. Shao, M. I. Hoopes, D. Luo, B. Ahsan, V. M. Grigoryants, W. Song, H. Huang, G. Zhang, R. K. Pandey, J. Geng, B. A. Pfeifer, C. P. Scholes, J. Ortega, M. Karttunen and J. F. Lovell, *Nat Commun* **2014**, *5*, 3546.
[21] a) I. Rizvi, G. Obaid, S. Bano, T. Hasan and D. Kessel, *Lasers Surg Med* **2018**, *50*, 499-505; b) G. Obaid, W. Jin, S. Bano, D. Kessel and T. Hasan, *Photochem Photobiol* **2018**.
[22] L. G. Parratt, *Physical Review* **1954**, *95*, 359-369.
[23] A. Nelson, *Journal of Applied Crystallography* **2006**, *39*, 273-276.
[24] J. Massiot, A. Makky, F. Di Meo, D. Chapron, P. Trouillas and V. Rosilio, *Physical Chemistry Chemical Physics* **2017**, *19*, 11460-11473.
[25] D. M. Price, *Journal of Thermal Analysis* **1995**, *45*, 1285-1296.
[26] A. D. Bangham, M. M. Standish and J. C. Watkins, *J Mol Biol* **1965**, *13*, 238-252.
[27] M. M. da Cunha, S. Trepout, C. Messaoudi, T. D. Wu, R. Ortega, J. L. Guerquin-Kern and S. Marco, *Micron* **2016**, *84*, 23-36.
[28] T. J. Underwood, M. F. Derouet, M. J. White, F. Noble, K. A. Moutasim, E. Smith, P. A. Drew, G. J. Thomas, J. N. Primrose and J. P. Blaydes, *Biol Cell* **2010**, *102*, 635-644.
[29] Y. Shimada, M. Imamura, T. Wagata, N. Yamaguchi and T. Tobe, *Cancer* **1992**, *69*, 277-284.
[30] S. Bolte and F. P. Cordelieres, *Journal of Microscopy-Oxford* **2006**, *224*, 213-232.
[31] a) R. Rosseto and J. Hajdu, *Chem Phys Lipids* **2010**, *163*, 110-116; b) R. Rosseto and J. Hajdu, *Tetrahedron* **2014**, *70*, 3155-3165.
[32] E. J. O'Neil, K. M. DiVittorio and B. D. Smith, *Org Lett* **2007**, *9*, 199-202.
[33] R. Bittman and C. A. Verbicky, *J Lipid Res* **2000**, *41*, 2089-2093.
[34] a) J. F. Nagle and S. Tristram-Nagle, *Biochimica et Biophysica Acta (BBA) - Reviews on Biomembranes* **2000**, *1469*, 159-195; b) B. A. Lewis and D. M. Engelman, *Journal of Molecular Biology* **1983**, *166*, 211-217.
[35] D. Luo, N. Li, K. A. Carter, C. Lin, J. Geng, S. Shao, W. C. Huang, Y. Qin, G. E. Atilla-Gokcumen and J. F. Lovell, *Small* **2016**, *12*, 3039-3047.
[36] J. N. Israelachvili, *Intermolecular and Surface Forces*, **2011**, p. 538-542
[37] V. V. Kumar, *Proc Natl Acad Sci U S A* **1991**, *88*, 444-448.
[38] a) A. Seelig, *Biochim Biophys Acta* **1987**, *899*, 196-204; b) H. Fischer, R. Gottschlich and A. Seelig, *J Membr Biol* **1998**, *165*, 201-211.
[39] W. Humphrey, A. Dalke and K. Schulten, *Journal of Molecular Graphics* **1996**, *14*, 33-38.
[40] J. T. Davies and E. K. Rideal in *Interfacial Phenomena*, *Vol.* Academic Press: New York and London, **1963**.
[41] M. J. Griffith, M. James, G. Triani, P. Wagner, G. G. Wallace and D. L. Officer, *Langmuir* **2011**, *27*, 12944-12950.
[42] a) J. Majewski, T. L. Kuhl, K. Kjaer and G. S. Smith, *Biophysical Journal* **2001**, *81*, 2707-2715; b) M. Broniatowski, M. Flasinski, P. Dynarowicz-Latka and J. Majewski, *Journal of Physical Chemistry B* **2010**, *114*, 9474-9484.

[43] A. Korytowski, W. Abuillan, A. Makky, O. Konovalov and M. Tanaka, *J Phys Chem B* **2015**, *119*, 9787-9794.
[44] a) M.-C. Desroches, A. Kasselouri, M. Meyniel, P. Fontaine, M. Goldmann, P. Prognon, P. Maillard and V. Rosilio, *Langmuir* **2004**, *20*, 11698-11705; b) M.-H. Ropers and G. Brezesinski, *Soft Matter* **2013**, *9*, 9440-9448.
[45] K. Sabatini, J.-P. Mattila, F. M. Megli and P. K. J. Kinnunen, *Biophysical Journal* **2006**, *90*, 4488-4499.
[46] a) K. K. Ng, M. Takada, K. Harmatys, J. Chen and G. Zheng, *ACS Nano* **2016**, *10*, 4092-4101; b) M. Shakiba, K. K. Ng, E. Huynh, H. Chan, D. M. Charron, J. Chen, N. Muhanna, F. S. Foster, B. C. Wilson and G. Zheng, *Nanoscale* **2016**, *8*, 12618-12625; c) L. Cui, D. Tokarz, R. Cisek, K. K. Ng, F. Wang, J. Chen, V. Barzda and G. Zheng, *Angew Chem Int Ed Engl* **2015**, *54*, 13928-13932; d) K. K. Ng and G. Zheng, *Chemical Reviews* **2015**, *115*, 11012-11042.
[47] A. A. Krasnovsky, Jr., K. V. Neverov, S. Egorov, B. Roeder and T. Levald, *J Photochem Photobiol B* **1990**, *5*, 245-254.
[48] V. Rapozzi, M. Miculan and L. E. Xodo, *Cancer Biology & Therapy* **2009**, *8*, 1318-1327.
[49] a) C. S. Oliveira, R. Turchiello, A. J. Kowaltowski, G. L. Indig and M. S. Baptista, *Free Radical Biology and Medicine* **2011**, *51*, 824-833; b) A. P. Thomas, L. Palanikumar, M. T. Jeena, K. Kim and J.-H. Ryu, *Chemical Science* **2017**, *8*, 8351-8356; c) C.-J. Zhang, Q. Hu, G. Feng, R. Zhang, Y. Yuan, X. Lu and B. Liu, *Chemical Science* **2015**, *6*, 4580-4586.
[50] a) P. M.-K. Tang, X.-Z. Liu, D.-M. Zhang, W.-P. Fong and K.-P. Fung, *Cancer Biology & Therapy* **2009**, *8*, 533-539; b) W.-Y. Lee, D.-S. Lim, S.-H. Ko, Y.-J. Park, K.-S. Ryu, M.-Y. Ahn, Y.-R. Kim, D. W. Lee and C.-W. Cho, *Journal of Photochemistry and Photobiology B: Biology* **2004**, *75*, 119-126.